J. Fluid Mech. (2013), *vol.* 717, *pp.* 322–346.
doi:10.1017/jfm.2012.574

Dynamics of the large-scale circulation in high-Prandtl-number turbulent thermal convection

Yi-Chao Xie, Ping Wei and Ke-Qing Xia†

Department of Physics, The Chinese University of Hong Kong, Shatin, Hong Kong, China

(Received 27 June 2012; revised 22 October 2012; accepted 17 November 2012;
first published online 1 February 2013)

We report experimental investigations of the dynamics of the large-scale circulation (LSC) in turbulent Rayleigh–Bénard convection at high Prandtl number $Pr = 19.4$ (and also $Pr = 7.8$) and Rayleigh number Ra varying from 8.3×10^8 to 2.9×10^{11} in a cylindrical convection cell with aspect ratio unity. The dynamics of the LSC is measured using the multithermal probe technique. Both the sinusoidal-fitting (SF) and the temperature-extrema-extraction (TEE) methods are used to analyse the properties of the LSC. It is found that the LSC in high-Pr regime remains a single-roll structure. The azimuthal motion of the LSC is a diffusive process, which is the same as those for Pr around 1. However, the azimuthal diffusion of the LSC, characterized by the angular speed Ω is almost two orders of magnitude smaller when compared with that in water. The non-dimensional time-averaged amplitude of the angular speed $\langle|\Omega|\rangle T_d$ ($T_d = L^2/\kappa$ is the thermal diffusion time) of the LSC at the mid-height of the convection cell increases with Ra as a power law, which is $\langle|\Omega|\rangle T_d \propto Ra^{0.36\pm0.01}$. The Re number based on the oscillation frequency of the LSC is found to scale with Ra as $Re = 0.13Ra^{0.43\pm0.01}$. It is also found that the normalized flow strength $\langle\delta\rangle/\Delta T \times Ra/Pr \propto Re^{1.5\pm0.1}$, with the exponent in good agreement with that predicted by Brown & Ahlers (*Phys. Fluids*, vol. 20, 2008, p. 075101). A wealth of dynamical features of the LSC, such as the cessations, flow reversals, flow mode transitions, torsional and sloshing oscillations are observed in the high-Pr regime as well.

Key words: Bénard convection, plumes/thermals, turbulent convection

1. Introduction

Thermal convection is a phenomenon occurring widely in both nature and industrial processes. Turbulent Rayleigh–Bénard (RB) convection, which is a fluid layer confined between two horizontally parallel plates with heated bottom plate and cooled top plate, has become an idealized model to study the thermal convection problem experimentally, numerically and theoretically. The system is controlled by three parameters, namely the Rayleigh number $Ra = \alpha g \Delta T H^3/(\nu\kappa)$, the Prandtl number $Pr = \nu/\kappa$ and the aspect ratio $\Gamma = D/H$, where α is the thermal expansion coefficient, g the gravitational acceleration, ΔT the temperature difference between the top and

† Email address for correspondence: kxia@phy.cuhk.edu.hk

bottom plates, H the height of the fluid layer between the plates, D the diameter of the convection cell and ν and κ are the kinematic viscosity and the thermal diffusivity of the convecting fluid, respectively. The emergence of a coherent large-scale circulation (LSC), also called the mean wind, which is a quasi-two-dimensional (quasi-2D) fly wheel structure, when the system is in the hard-turbulence regime over a turbulent background has attracted a lot of interest.

Using water and gas, respectively, as the working fluids with moderate and low Pr numbers, the dynamics of the LSC has been studied extensively (see, e.g. Brown, Nikolaenko & Ahlers 2005; Sun, Xi & Xia 2005*a*; Xi, Zhou & Xia 2006; Xi & Xia 2007, 2008*a*,*b*; Ahlers *et al.* 2009*a*; Ahlers, Grossmann & Lohse 2009*b*). Qiu & Tong (2001) studied the large-scale velocity structures using the laser Doppler velocimetry (LDV) technique in a water-filled convection cell, and found that the velocity field inside the convection cell could be classified into three regions. One is the thin viscous boundary layer region, the second is the central core region with constant mean velocity gradient and the third is the intermediate plume-dominated area, which has very strong fluctuations. Xi, Lam & Xia (2004) studied the onset of the LSC using the shadow graph and the particle image velocimetry (PIV) techniques. They found that the emergence of a large coherent flow structure indeed is a result of the self-organization of the thermal plumes which erupt from the top and bottom thermal boundary layers and that it is the thermal plumes that sustain the LSC. Further experimental measurements of the velocity field by Sun, Xia & Tong (2005*b*) using the PIV technique showed how the convecting fluid in different regions of the cell interact to generate a synchronized and coherent motion in this closed system.

By the virtue that the LSC carries the up-rising hot and down-going cold plumes, the azimuthal orientation and flow strength of the LSC could be determined by measuring the temperature distribution along a perimeter at fixed height of a cylindrical cell. Cioni, Ciliberto & Sommeria (1997) first used this method to measure the dynamics of the LSC. Later on, a similar method, which is called the multithermal probe technique, was used to study the dynamics of the LSC (Brown & Ahlers 2006*b*; Sun & Xia 2007; Xi & Xia 2007, 2008*a*,*b*). These include the azimuthal meandering of the nearly vertical circulation plane (reorientations), the momentary vanishing of the flow strength (cessations), the change of the flow direction by π either as a result of cessation events or by the azimuthal orientations (flow reversals). It has also been found that the flow configuration strongly depends on the aspect ratio Γ of the convection cell (Xi & Xia 2008*b*; Weiss & Ahlers 2011). This change of flow configuration is called a flow mode transition. One of the typical flow mode transitions is the single-roll mode to double-roll mode to single-roll mode (SRM–DRM–SRM), which is more likely to occur in cells with aspect ratio smaller than one. Recently, it is found that the global heat transport efficiency, namely the Nusselt number Nu, depends on the internal flow modes of the LSC (Xi & Xia 2008*b*; Weiss & Ahlers 2011; Xia 2011).

Another very intriguing feature in turbulent RB convection is the periodic oscillation of the LSC near the top and bottom plates with a phase delay of π in a cylindrical cell (Funfschilling & Ahlers 2004), which is called the torsional oscillation. Moreover, it has been found recently that LSC exhibits a horizontal periodic displacement at the mid-height of the cell, perpendicular to its circulation plane, which is referred to as the sloshing oscillation of the LSC (Xi *et al.* 2009; Zhou *et al.* 2009). In addition it has been long observed that there exists a low-frequency oscillation of both the temperature and velocity field of the turbulent RB convection (Castaing *et al.* 1989; Sano, Wu & Libchaber 1989; Takeshita *et al.* 1996; Ashkenazi & Steinberg

1999; Niemela *et al.* 2001; Shang & Xia 2001). It is now known that the origin of these oscillations is the sloshing oscillation of the bulk fluid plus the torsional oscillation of the top and bottom parts of the LSC (Xi *et al.* 2009; Zhou *et al.* 2009). Based on this characteristic oscillation frequency, a Reynolds number Re can be defined as $Re = LHf/\nu$, where L is a characteristic length scale of the LSC and f the oscillation frequency of either the velocity field or the temperature field (Grossmann & Lohse 2002; Brown, Funfschilling & Ahlers 2007). The key issue is how Re scales with the system control parameters, i.e. what is the functional form of $Re(Ra, Pr)$. Varieties of experimental data of this scaling were given by Sun & Xia (2005) and Brown *et al.* (2007). There are also theoretical studies of the scaling behaviour of turbulent RB convection. The predictions of the model proposed by Grossmann & Lohse (2000, 2001, 2002) have found good agreements with most of the experimental data on the scaling of both $Nu(Ra, Pr)$ and $Re(Ra, Pr)$.

All of the properties of the LSC mentioned above are investigated with a very wide range of Ra. While the effects of Prandtl number Pr are studied much less. Using four kinds of fluids of different Pr, Lam *et al.* (2002) made experimental measurements of the viscous boundary layer and Re. Their results yielded scaling relationships of the viscous boundary layer thickness δ_v and of Re with respect to Ra (from 1×10^8 to 3×10^{10}) and Pr (from 3 to 1205) are $\delta_v/H = 0.65Pr^{0.24}Ra^{-0.16}$ and $Re = 1.1Ra^{0.43}Pr^{-0.76}$, respectively. However, to the best of the authors' knowledge, the dynamics of the LSC in turbulent RB convection is studied only in a limited range of Pr from 0.7 to 5.3. Using gas as the working fluid in a convection cell with an aspect ratio of one half, Ahlers *et al.* (2009*a*) measured both the heat transport efficiency and the dynamics of the LSC at $Pr = 0.67$. They achieved Ra up to 10^{13} and found that the LSC could survive to the highest Ra in their experiment. They also reported the relatively long vanishings of the flow strength, which are different from cessations such as those found in turbulent RB convection using water as the working fluid. However, the dynamics of the LSC in high-Pr regime has not yet been investigated, which is the subject of the present study.

The reminder of this paper is organized as follows. First the experimental setup and data analysis methods are introduced in § 2. Section 3 presents the main results of our experiments. In § 3.1 we present the general features of the LSC; in § 3.2 we present the azimuthal rotations of the LSC; in § 3.3 we present the measured Reynolds number Re and a comparison of our results with earlier experiments and also model predications; in § 3.4 we present the dynamical behaviours of the LSC, such as cessations, flow reversals, flow mode transitions as well as the twisting and sloshing oscillations. Our findings are summarized and concluded in § 4. Examples of flow reversals and flow mode transitions are given in appendix A. The power spectra of the temperature and also the azimuthal orientation of the LSC, from which we identify the twisting and sloshing oscillations, are given in appendix B.

2. Experimental setup and data analysis methods

2.1. *The convection cell and working fluids*

A cylindrical convection cell with an aspect ratio close to unity, height $H = 19.3$ cm and diameter $D = 19.0$ cm was used in the experiments. Two copper plates 1.0 cm thick with a nickel-coated surface were used as the heating and cooling plates. An electrical heater was sandwiched in the bottom plate as a heating source and the top plate was connected to a recirculating cooler as cooling source. The temperature of

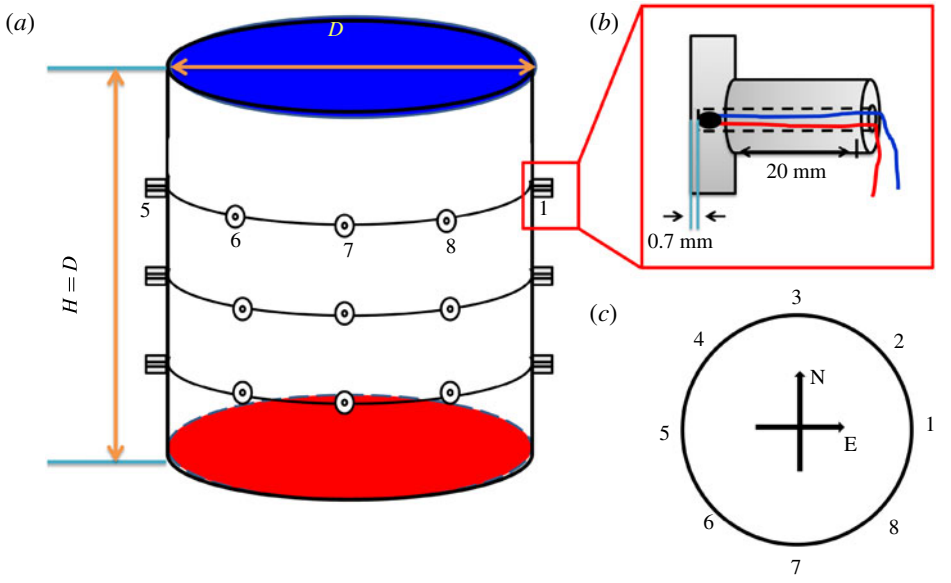

FIGURE 1. (Colour online) Schematic drawing of the experimental setup. (*a*) The sidewall of the convection cell with thermistor holders used in experiments. The numbers 1–8 indicate the azimuthal position of the thermistors, which is shown in (*c*) with indications of the north (N) and east (E) directions in the lab frame when viewed from the top of the cell. (*b*) The dimension of the thermistor holder. The distance between the fluid sidewall interface and the end of the hole in the holder is 0.7 mm.

the top and bottom plates were monitored by eight thermistors with four embedded in each plate. The largest temperature difference measured by the thermistors in the same plate was within 1.5 % of the temperature difference ΔT between the top and bottom plates. The convection cell was wrapped by three layers of Styrofoam to prevent heat loss.

In order to measure the horizontal temperature profile induced by the LSC, tiny hollow cylinders with length $L = 20.0$ mm, outer diameter $D_{outer} = 10.0$ mm and inner diameter $D_{inner} = 2.5$ mm were adhered to the sidewall as holders of the thermistors to obtain a snug fit of the thermistors to the sidewall (see figure 1 for detail). Three heights of thermistor holders located at distances $H/4, H/2$ and $3H/4$ from the bottom plate, which we denoted as the bottom, middle and top heights of the LSC, respectively, were used. The three levels of thermistor holders were distributed uniformly in eight columns around the sidewall and numbered 1–8 (figure 1*a,c*). A total of 24 thermistors (Omega Inc., Model 44031) with an accuracy of 0.01 °C and head diameter 2.4 mm were placed inside the holders to measure the horizontal temperature profiles. The sampling rate of the temperature profiles was 0.37 Hz. The convection cell was levelled to within 0.001 rad in the experiments.

Water and fluorinert FC-77 electronic liquid (3M Company, hereafter referred as FC77) were used as the working fluids. Since water is a very commonly used fluid, we will only mention the physical properties of FC77. The density of FC77 is 1780 kg m^{-3} and its kinematic viscosity is 7.2×10^{-7} m^2 s^{-1} at 40 °C. For other physical properties, we refer to the MSDS data sheet published by 3M Company. As the physical properties of fluids are a function of temperature, in the experiments these

properties are calculated based on the bulk temperature of the fluids. For experiments using water as the working fluid, the Prandtl number is $Pr = 7.8$ and Ra is from 8.3×10^8 to 1.1×10^9. For experiments using FC77 as the working fluid, the Prandtl number is $Pr = 19.4$. By varying the temperature difference ΔT between the top and bottom plates, we are able to vary the Rayleigh number Ra from 1.3×10^{10} to 2.9×10^{11} for FC77, which corresponds to ΔT from 2.44 to 53.69 °C. The measurement periods for different runs varied from 50–700 h.

2.2. *Multithermal probe technique*

The multithermal probe technique is first introduced by Cioni *et al.* (1997). The principle is that the LSC carries the hot (cold) plumes erupted from the bottom (top) thermal boundary layer (Xi *et al.* 2004), and thus causes a higher (lower) temperature along its path than the surrounding fluid at a horizontal height. By measuring the temperature profile at a horizontal height of the convection cell, the signature, e.g. the azimuthal position of the hot (cold) plumes and thus the azimuthal position of the LSC, can be detected. The contrast between the hottest and coldest temperature is a measure of the flow strength inside the convection cell. If the flow is very strong, it will cause a larger temperature difference of the hot and cold sides of the LSC. Thus, the measured temperature contrast will be larger. By choosing a reference position along the azimuthal direction at a certain horizontal height of the cell, the azimuthal position of the LSC can be determined.

2.3. *Data analysis method*

The sinusoidal-fitting (SF) and the temperature-extrema-extraction (TEE) methods are applied in the data analysis. For the SF method, the measured temperature profile of a certain horizontal height is fitted to a cosine function

$$T_i = T_0 + \delta \cos\left(\frac{\pi}{4} i - \theta\right), \quad (i = 0 \ldots 7) \tag{2.1}$$

where T_i is the temperature reading of the ith thermistor, T_0 is the mean temperature of all of the eight thermistors, δ is the magnitude of the cosine function which is a measure of the flow strength of the LSC and θ is the azimuthal position where the hot ascending plumes of the LSC rise, which we denote as the azimuthal orientation of the LSC.

We show in figure 2 an example of the measured horizontal temperature profiles and the fitting results. The symbols are the experimental data and lines are the sinusoidal fitting results. It is seen that the cosine functions could represent the data very well.

The TEE method, which is first introduced by Xi *et al.* (2009) and described in detail by Zhou *et al.* (2009), is used to study the sloshing oscillation of the LSC. The off-centre distance of the LSC's central line d, which is a characterization of the sloshing motion, is defined as the distance between the mid-point of the central line and the centre of a horizontal plane of the cylindrical sidewall. The normalized d is given by

$$d/D = \tfrac{1}{2} \cos\left(\tfrac{1}{2}(\theta_{max} - \theta_{min})\right) \tag{2.2}$$

where θ_{max} and θ_{min} are the azimuthal positions of the highest and lowest temperatures, respectively.

It has been shown that the SF method and the TEE method basically provide the same information about δ and θ (Zhou *et al.* 2009). Thus, in the following sections,

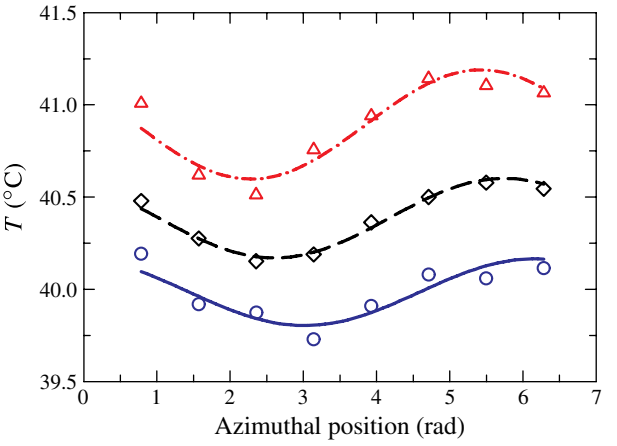

FIGURE 2. (Colour online) An example of instantaneous temperature profiles measured by the three heights of thermistors ($Ra = 2.0 \times 10^{11}$ and $Pr = 19.4$). The curves are sinusoidal fittings to the data. The circles, diamonds and triangles represent the horizontal temperature profiles of the top, middle and bottom heights of the LSC, respectively.

except for discussing the sloshing oscillations, we use data obtained by the SF method during all of the analysis of the dynamics of the LSC.

3. Results and discussion

As results obtained in water at $Pr = 7.8$ exhibit similar features to those obtained from FC77 at $Pr = 19.4$, in this section we will mostly present results obtained from FC77, unless stated otherwise. The water results are presented mainly in § 3.4 when we discuss the cessation statistics.

3.1. *General features of the LSC*

The general features of the LSC are revealed by studying the respective cross-correlation functions of the flow strength δ (the azimuthal orientation θ) between different heights and the probability distribution function (p.d.f.) of δ (also θ) at different heights.

Figure 3 shows a short time segment of the measured δ and θ at three different heights. It is seen that the flow strength of the three heights remains well above zero during this period. At the same time, the azimuthal orientation at different heights are close to each other. Also we note that both the flow strength and orientation of different heights have similar fluctuations. In order to characterize this similarity, we calculate the long-time cross-correlation functions of both the flow strength δ and orientation θ between different heights of the LSC. The cross-correlation function of two time series $A(t)$ and $B(t)$ is defined as

$$C_{A,B}(\tau) = \frac{\langle [A(t+\tau) - \langle A \rangle][B(t) - \langle B \rangle] \rangle}{\sigma_A \sigma_B} \tag{3.1}$$

where $\langle \cdots \rangle$ represents the corresponding time-averaged value and σ_A, σ_B are the standard deviation of the time series A and B, respectively. When $A = B$, C_{AB} is the auto-correlation function and we denote this as C_{AA}.

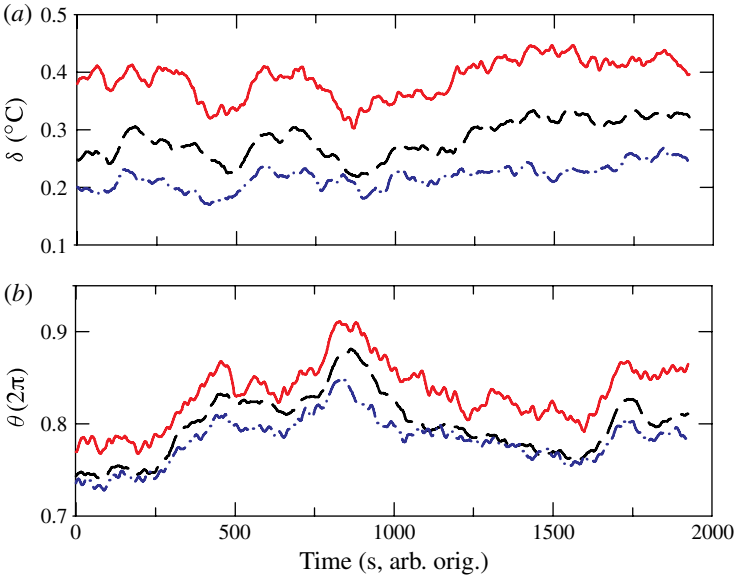

FIGURE 3. (Colour online) A time segment of the measured (*a*) flow strength δ and (*b*) azimuthal orientation θ of the LSC ($Ra = 2.0 \times 10^{11}$ and $Pr = 19.4$). In both figures, the dash-dotted, dashed and solid lines represent δ or θ measured from the top, middle and bottom heights of the LSC, respectively.

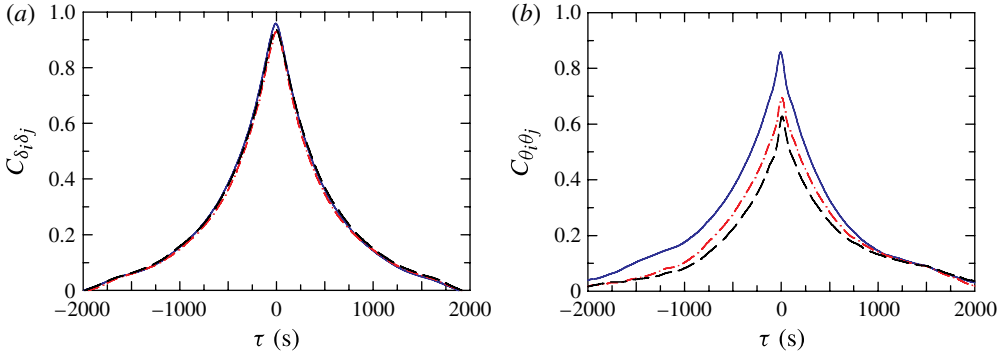

FIGURE 4. (Colour online) Cross-correlation functions of: (*a*) the flow strength δ and (*b*) orientation θ of the LSC at different heights ($Ra = 2.0 \times 10^{11}$ and $Pr = 19.4$). In both figures, the solid, dash-dotted and dashed lines are the cross-correlation function of the corresponding quantities between the top and middle, middle and bottom, and top and bottom heights of the LSC, respectively.

Figure 4 shows the cross-correlation functions of the flow strength (*a*) and the orientation (*b*) between different heights (here $ij = tm$, tb and mb which corresponds to the quantities from top and middle, top and bottom, middle and bottom heights of the LSC, respectively). From figure 4(*a*), we see that the C_{δ_t,δ_m}, C_{δ_t,δ_b} and C_{δ_m,δ_b} essentially collapse together with a correlation coefficient close to one at time lag $\tau = 0$, which implies that the flow strength measured at different heights of the LSC are strongly

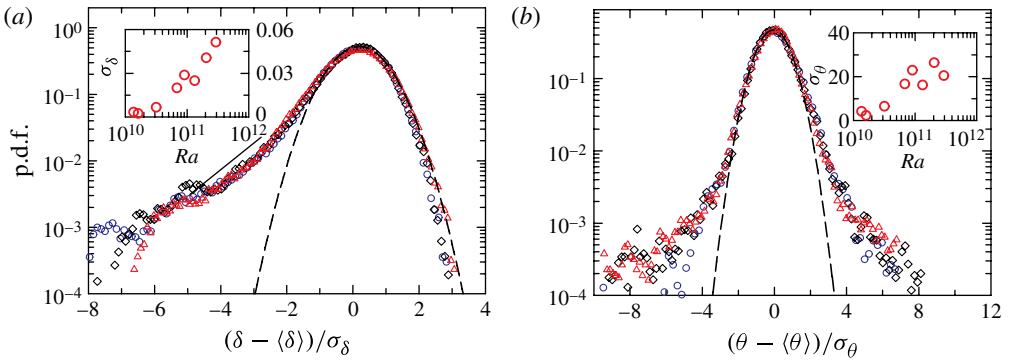

FIGURE 5. (Colour online) Probability distribution functions of (*a*) the normalized flow strength and (*b*) the normalized orientation of the LSC ($Ra = 2.0 \times 10^{11}$ and $Pr = 19.4$). The standard deviation of the flow strength σ_δ (in units of °C) and that of the orientation σ_θ (in units of degrees) measured from the mid-height are shown as insets of (*a,b*), respectively. The solid curve in (*a*) marks the exponential distribution. The dashed curve in (*a,b*) represents a Gaussian distribution function with the same variance as the corresponding data for reference. In both figures, the circles, diamonds and triangles represent the p.d.f.s of the corresponding quantities measured from the top, middle and bottom heights of the LSC, respectively.

correlated with each other without time delay. Figure 4(*b*) shows that C_{θ_t,θ_m}, C_{θ_t,θ_b} and C_{θ_m,θ_b} have a strong positive correlation coefficient above 0.65 at time lag $\tau = 0$, which also indicates that the azimuthal orientations of different heights of the LSC correlate with each other with no time delay. For the other *Ra* investigated in the experiments, these strong positive correlations of δ (also θ) between different heights of the LSC are also found.

Figure 5 shows the p.d.f.s of $(\delta - \langle\delta\rangle)/\sigma_\delta$ (*a*) and those of $(\theta - \langle\theta\rangle)/\sigma_\theta$ (*b*) of the LSC at different heights, where $\langle\cdots\rangle$ denotes the mean value. σ_δ and σ_θ are the respective standard deviation of δ and θ. These figures show that the p.d.f.s of δ and θ at different heights collapse on top of each other except for the tails, which have a lower probability. From the p.d.f.s of δ at different heights, we see that the p.d.f.s deviate far away from a Gaussian distribution (dashed line in the figure) at the left tail while the right tail is in good agreement with a Gaussian distribution. The exponential-like tails (the solid line in figure 5(*a*) is a mark of exponential distribution as reference) tell that it is more probable for the flow strength to be below the mean flow strength and these tails are corresponding to the time period when there are cessations, reversals or flow mode transitions, during which δ is relatively low. The asymmetric p.d.f.s of δ are quite different from those of the θ, which are shown in figure 5(*b*). It shows that there is a preferred orientation for the LSC, which we denote as $\langle\theta\rangle$. For different *Ra* in the experiments, we found that the preferred orientation of the LSC varies from 4.23 to 6.24 rad with no apparent trend. Thus, we suspect it is not the asymmetry of the convection cell other than through some physical effect that causes the symmetry breaking of the system. We also found no apparent dependence of $\langle\theta\rangle$ on any particular features of the cell, for example the location of the inlets and outlets of cooling water. One of the possible reasons is the effect of the Earth's Coriolis force as discussed by Brown & Ahlers (2006*a*). Similar results have been observed at moderate *Pr* using water as the working fluid (Brown & Ahlers 2006*a*; Xi & Xia 2008*a*).

It is also seen from the figure that the p.d.f.s of θ are approximately Gaussian distributed for small fluctuations. While for fluctuations larger than $\sim 3\sigma_\theta$, the probabilities are larger than those given by the Gaussian distribution and have exponential-like tails. Also shown as insets of the figures are the standard deviations of δ and θ obtained at the middle height of the LSC. For σ_δ, we can see that with the increase of Ra, σ_δ increases dramatically. The standard deviation σ_θ shows no Ra dependence except for the two lowest Ra, in which case, due to the low ΔT, the thermal probes cannot detect the azimuthal position of the LSC very well. Similar results were reported by Xi *et al.* (2006) using water as the working fluid at $Pr = 5.3$.

For the Pr and Ra covered in the present experiments, we observe similar results of the statistics. These results imply that the flow strength δ and the orientation θ at different heights of the LSC strongly correlate with each other and they share essentially the same p.d.f., which indicates that the LSC in a cell with aspect ratio unity and cylindrical geometry, is a single-roll structure in the high-Pr regime.

3.2. *The azimuthal rotations of the LSC*

The dynamics of the azimuthal motion of the LSC is a diffusive process (Sun *et al.* 2005*a*). According to the observed statistical behaviour, there are several models attempting to explain this phenomenon (Benzi 2005; Brown & Ahlers 2007, 2008). This azimuthal rotation of the LSC can be revealed by studying the angular speed Ω, which is the time derivative of θ. Since there are sudden change of θ from 0 to 2π and vice versa, using θ to define the angular speed of LSC will introduce some artificial errors. In order to eliminate this error, we define continuous variable $\phi_i = \theta_i \pm n \times 2\pi$ $(n = \ldots, -1, 0, 1, \ldots)$. The anticlockwise direction is defined as positive and that of the clockwise direction is defined as negative when viewed from the top of the cell. Then we define the angular speed as follows

$$\Omega_i = \frac{\mathrm{d}\phi_i}{\mathrm{d}t} = \frac{\phi_i(t+\epsilon) - \phi_i(t)}{\epsilon} \tag{3.2}$$

where ϵ is the sampling time step of the orientation and $i = t, m$ and b, which stand for the top, middle and bottom heights of the LSC.

A time segment of the measured angular speed Ω at different heights is shown in figure 6(*a*). The LSC moves very slowly along the azimuthal direction, which is of the order of 10^{-3} rad s^{-1}. We also calculate the amplitude of the angular speed Ω_m using data from Xi & Xia (2008*a*) with water as the working fluid at $Pr = 5.3$. The results of Xi & Xia (2008*a*) yield an angular speed of the order of 10^{-1} rad s^{-1}. Thus, it is clear that the angular speed at $Pr = 19.4$ is roughly two orders of magnitude smaller than that at $Pr = 5.3$. We note that the sampling rate of the azimuthal orientation θ in Xi & Xia (2008*a*) is 0.29 Hz and that of the present experiment is 0.37 Hz, which is comparable with that of Xi & Xia (2008*a*). Thus, the difference of the angular speed is not caused by the finite sampling rate of θ.

Another way to quantify the azimuthal diffusion is to determine the azimuthal diffusion constant D_Ω of the LSC. We plot the mean-square change $\langle(\mathrm{d}\Omega)^2\rangle$ as a function of the time interval $\mathrm{d}t$ in figure 7, where $\mathrm{d}\Omega = \Omega(t + \mathrm{d}t) - \Omega(t)$. From figure 7 we obtain a diffusion constant $D_\Omega = 3.2 \times 10^{-7}$ rad^2 s^{-3} of the angular speed at $Pr = 19.4$ and $Ra = 2.00 \times 10^{11}$. Brown & Ahlers (2008) reported that the azimuthal diffusivity of the angular speed D_Ω is 2.9×10^{-5} rad^2 s^{-3} at $Ra = 1.1 \times 10^{10}$ and $Pr = 4.38$ and that D_Ω scales with Ra as $D_\Omega \propto Ra^{0.76}$. Thus, for $Ra = 2.0 \times 10^{11}$ and $Pr = 4.38$, we can estimate that D_Ω is 2.6×10^{-4} rad^2 s^{-3}. Again we find that

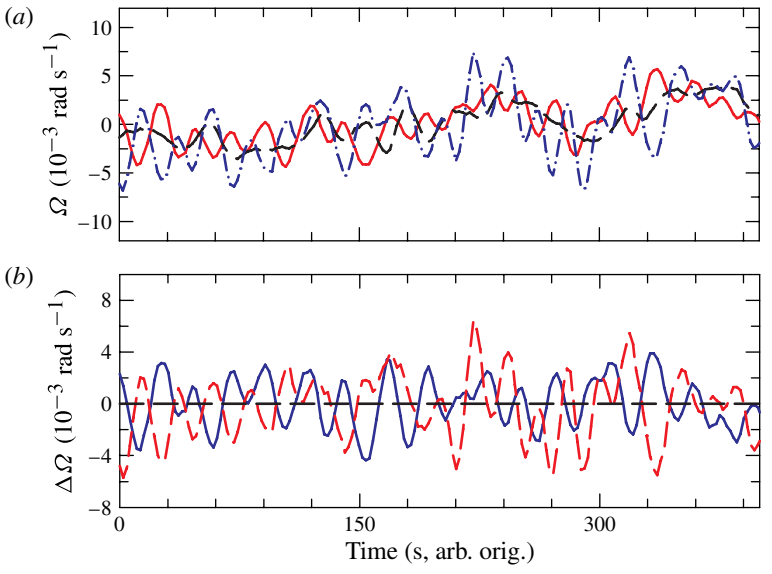

FIGURE 6. (Colour online) (*a*) A time segment showing the measured angular speed Ω of the LSC ($Ra = 2.0 \times 10^{11}$ and $Pr = 19.4$). The dash-dotted, dashed and solid lines are Ω of the top, middle and bottom heights of the LSC, respectively. (*b*) The antiphase motion of the top and bottom heights of the LSC (calculated from the same data sets as in (*a*)) with the Ω from the middle height as reference. The solid and dashed lines are $\Delta\Omega_{tm}$ and $\Delta\Omega_{bm}$, respectively.

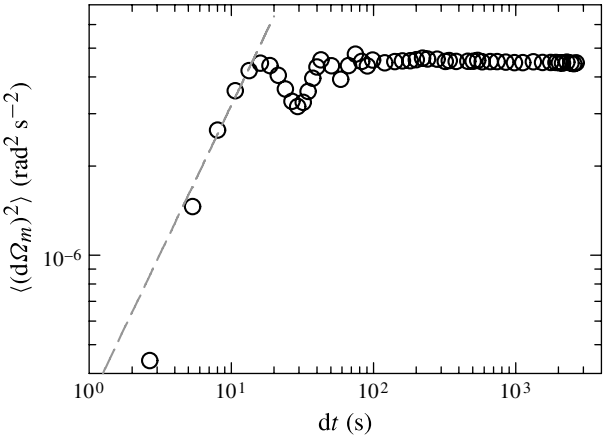

FIGURE 7. The mean-square change of the angular speed $\langle(\mathrm{d}\Omega)^2\rangle$ (circles) as a function of the time interval $\mathrm{d}t$ ($Ra = 2.0 \times 10^{11}$ and $Pr = 19.4$). The dashed line is a fit of $\langle(\mathrm{d}\Omega)^2\rangle = D_\Omega\,\mathrm{d}t$ for $2.7 \leqslant \mathrm{d}t \leqslant 10.7$ s, which yields $D_\Omega = 3.2 \times 10^{-7}$ rad^2 s^{-3}.

the diffusivity of the present results at $Pr = 19.4$ is almost three orders of magnitude smaller than that at $Pr = 4.38$.

In the present experiment, the convection cell is levelled to within 0.001 rad. It has been shown that this levelling will not lock the direction of LSC (Xi & Xia 2008*b*).

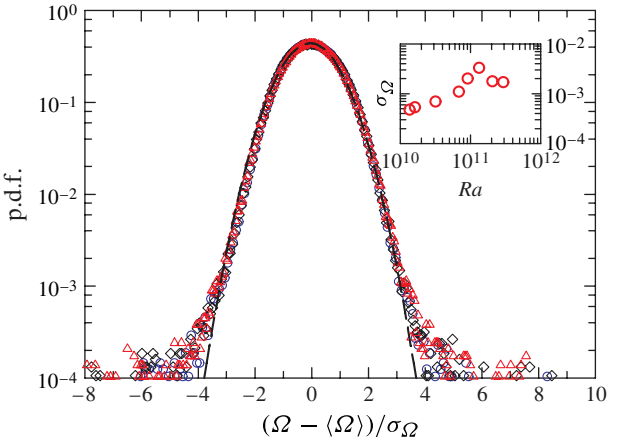

FIGURE 8. (Colour online) Probability distribution functions of the normalized angular speed of the LSC at three different heights ($Ra = 2.0 \times 10^{11}$ and $Pr = 19.4$). The inset shows the standard deviation σ_Ω (in units of rad s^{-1}) at the middle height. The circles, diamonds and triangles represent the p.d.f. of Ω measured from the top, middle and bottom heights of the LSC, respectively. The dashed curve represents a Gaussian distribution function with the same variance as the corresponding data.

Thus, we speculate that the relatively slow azimuthal motion of the LSC at high Pr is not due to the imperfect levelling of the convection cell. According to the LSC model proposed by Brown & Ahlers (2007), the damping of the azimuthal motion of the LSC comes from either viscosity or the rotational inertia of the LSC in its circulation plane. The kinematic viscosity of water and FC77 at temperature 40 °C is 6.58×10^{-7} m^2 s^{-1} and 5.69×10^{-7} m^2 s^{-1}, respectively. It is seen that they are comparable with each other. So the difference for these two Pr is not caused by the viscosity. For the rotational inertia, since the density of FC77 is almost twice that of water, the rotational inertia of the LSC in FC77 will be larger than in water in the same convection cell if we consider the LSC as a rigid rotator. Thus, it is more difficult for the LSC to move azimuthally in FC77 than in water.

Another intriguing phenomenon is the top and bottom heights of the LSC move out of phase with each other, which is revealed by looking into the angular speed at the top and bottom heights. In figure 6(*b*), we plot the angular speed of the LSC at top and bottom heights by subtracting the mean trend of Ω, which is Ω_m. We see that $\Delta\Omega_{tm} = \Omega_t - \Omega_m$ and $\Delta\Omega_{bm} = \Omega_b - \Omega_m$ oscillate around zero with π phase delay.

Figure 8 shows the p.d.f.s of $(\Omega - \langle\Omega\rangle)/\sigma_\Omega$ at different heights with a Gaussian distribution function as reference (the dashed line). An interesting finding is that the p.d.f.s of different heights are well-defined Gaussian distribution functions, which is consistent with stochastic properties of the azimuthal dynamics of the LSC. The standard deviation of the angular speed measured at the mid-height of the LSC σ_{Ω_m} versus Ra is shown as inset of figure 8, from which we see that with the increase of Ra, σ_{Ω_m} increases. However, for the larger Ra, σ_{Ω_m} seems to be saturated.

The auto-correlation functions of Ω_t, Ω_m and Ω_b and cross-correlation function between $\Delta\Omega_{tm}$ and $\Delta\Omega_{bm}$ are shown in figure 9 with the time lag τ normalized by the LSC turnover time τ_0 obtained from the power spectrum of the temperature signal measured in the top plate. From figure 9 we see that the oscillation period of C_{Ω_t,Ω_t}, C_{Ω_m,Ω_m} and C_{Ω_b,Ω_b} are the same with the LSC turnover time. The correlations

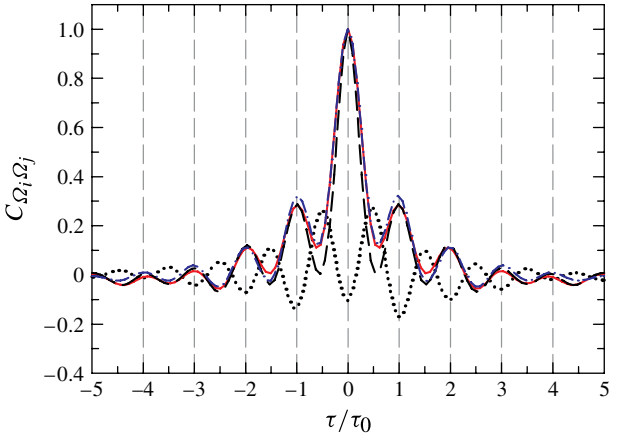

FIGURE 9. (Colour online) The auto-correlation functions of the angular speed of top (dashed line), middle (dash dot line) and bottom (solid line) heights of the LSC and the cross-correlation function of the angular speed of top and bottom heights (dot line) ($Ra = 2.0 \times 10^{11}$ and $Pr = 19.4$). Here τ_0 is the LSC turnover time obtained from the temperature power spectrum measured in the top plate.

of Ω at different heights last at least for $4\tau_0$. The strong correlations and oscillations of the auto-correlation functions indicate that the angular speed at different heights of the LSC oscillates in a periodic way together. From the cross-correlation function $C_{\Delta\Omega_{tm},\Delta\Omega_{bm}}$, we see that there is a negative peak at $\tau = 0$, which implies there is a π phase delay between them and this is indeed the case as we show in figure 6(*b*). Since the angular speed is a time derivative of the azimuthal orientation θ, we expect the angular speed to have the same oscillation frequency as that of θ, just like a pendulum. Owing to the relatively low signal-to-noise ratio of the present experiment, the torsional oscillation can hardly be observed from the cross-correlation function between θ_t and θ_b. However, from the above results and also the power spectra of θ_t, θ_m and θ_b (see appendix B), we confirm that the torsional oscillations of the LSC exist.

The time-averaged non-dimensional amplitudes of angular speed $\langle|\Omega_m|\rangle T_d$ measured at the middle height as a function of Ra for different Pr are shown in figure 10, where T_d is the thermal diffusion time scale defined as L^2/κ. Data from the present experiment at $Pr = 19.4$ are shown as circles and are multiplied by a factor of 270. The triangles are data obtained using the multithermal probe technique in a convection cell with aspect ratio unity using water as the working fluid at $Pr = 5.3$ (Xi & Xia 2008*b*). A power law fitting is attempted to the data, which yields the relation $\langle|\Omega_m|\rangle T_d \propto Ra^{0.36\pm0.01}$. We note that data at two different values of Pr have the same scaling exponent with respect to Ra.

3.3. *Reynolds number Re*

One important issue in the study of thermal turbulence is the scaling behaviour of the response parameters with the control parameters such as $Re = f(Ra, Pr, \Gamma)$ and $Nu = f(Ra, Pr, \Gamma)$. The experimental study of Nu dependence on Pr over a wide range of Ra was carried out by Xia, Lam & Zhou (2002) in a cylindrical cell with aspect ratio unity. Lam *et al.* (2002) also studied Re as a function of Ra and Pr using the same sets of fluids as Xia *et al.* (2002) used and their results of Re, which was defined using the typical oscillation frequency of the velocity

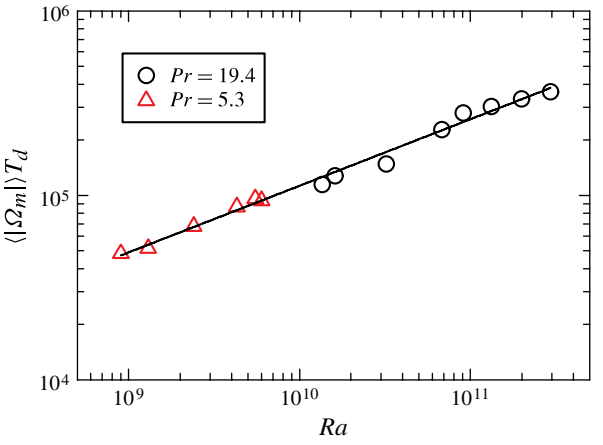

FIGURE 10. (Colour online) The measured non-dimensional time-averaged amplitude of the angular speed at the mid-height as a function of Ra at $Pr = 19.4$ (circles, present results) and $Pr = 5.3$ (triangles, data from Xi & Xia (2008*b*)). Here $T_d = L^2/\kappa$ is the thermal diffusion time. The solid line is a power law fit to the data yielding $\langle|\Omega_m|\rangle T_d \propto Ra^{0.36\pm0.01}$. In the figure, data for $Pr = 19.4$ are multiplied by a factor of 260.

field, show $Re = 1.1Ra^{0.43\pm0.01}Pr^{-0.76\pm0.01}$. Ashkenazi & Steinberg (1999) measured the velocity in turbulent RB convection using the LDV with gas as the working fluid. They found the relation of Re based on the characteristic oscillation frequency of the velocity power spectra with Ra and Pr is $Re = 2.6Ra^{0.43\pm0.02}Pr^{-0.75\pm0.02}$ with a shorter range of Pr compared with Lam *et al.* (2002). As we can see, these two experimental results agree with each other except that the prefactor of results from Ashkenazi & Steinberg (1999) is two times larger than that from Lam *et al.* (2002). The low-frequency oscillations of both the temperature and velocity field of the RB convection have been observed for a long time (Castaing *et al.* 1989; Sano *et al.* 1989; Takeshita *et al.* 1996; Ashkenazi & Steinberg 1999; Niemela *et al.* 2001; Shang & Xia 2001). It is now known that these oscillations are related to the periodic motion of the largest eddy in the system which is the LSC. Thus, based on this oscillation, we define a time scale $T_f = 1/f$, where f is the characteristic oscillation frequency obtained from the power spectra of either the temperature field or the velocity field. Choosing the characteristic length scale L of the LSC, the mean velocity of the LSC is defined as

$$U = L/T_f. \tag{3.3}$$

Based on different physical pictures, different L such as $\pi H, 4H, 2H$ are used in the literature. However, the results will only affect the prefactors of the power law relation of $Re = f(Ra, Pr)$. In the discussion below, since the LSC expands itself to the whole size of the cylindrical cell with aspect ratio unity, we choose $4H$ as the length scale. Then the Reynolds number Re is defined as

$$Re = \frac{UL}{\nu} = \frac{4H^2}{T_f\nu}. \tag{3.4}$$

Figure 11 is a plot of the measured Re as a function of Ra at $Pr = 19.4$. The circles are experimental data and solid line is a power law fitting to the data, which yields

$$Re = 0.13Ra^{0.43\pm0.01}. \tag{3.5}$$

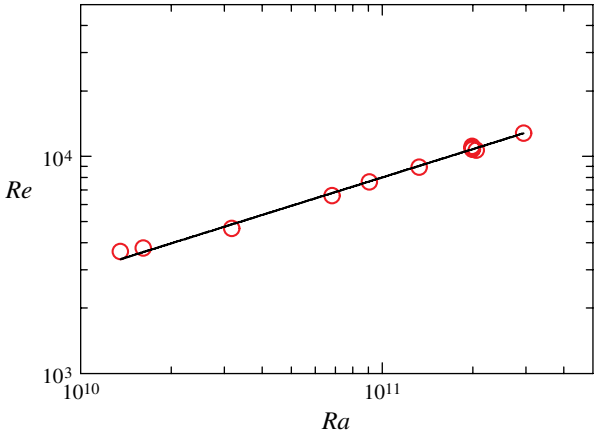

FIGURE 11. (Colour online) The measured Re based on the oscillation frequency of the LSC as a function of Ra. The solid line is a power law fit to the data yielding $Re = 0.13Ra^{0.43\pm0.01}$.

For the first sight, we see that the Ra scaling exponent of present experimental results is in good agreement with the experiments done by Lam *et al.* (2002) and Ashkenazi & Steinberg (1999). As the present case, the Pr is fixed, thus we substitute our Pr into the results by Lam *et al.* (2002) and obtain a relation $Re = 0.12Ra^{0.43\pm0.01}$. The prefactor is $\sim 8\,\%$ smaller than that of present results. Because Lam *et al.* (2002) used the typical velocity oscillation frequency while the oscillation frequency is obtained from the temperature field in our measurements, we see the two experiments agree with each other within experimental error, which confirms that the oscillations of the temperature field and the velocity field actually have the same origin as suggested by Xi *et al.* (2009). For the results of Ashkenazi & Steinberg (1999), the experiment was carried out in a cubic cell with square cross-section (76×76 mm^2) and height 107 mm. The different geometries of the convection cell will have different degree of confinements of the LSC (Zhou, Sun & Xia 2007; Kaczorowski *et al.* 2011). In the case of the cubic cell, the LSC is locked and always along the body diagonal of the cell. While in a cylindrical geometry, the LSC is free to move azimuthally. The confinements of the geometry of the convection cell may have some effects on the dynamics of the LSC. Another reason for the difference of prefactor of these two experimental results may be the aspect ratio effect. In the case of Ashkenazi & Steinberg (1999), the aspect ratio $\Gamma = D/H = 0.69$, while the aspect ratio in our experiment is close to unity. As suggested by Xi & Xia (2008*b*), the dynamics of the LSC has very strong dependence on the aspect ratio of the convection cell. Nevertheless, all of these experimental results of the Re scaling with respect to Ra agree very well with each other, which implies that there must be something in common of the dynamical properties of the LSC with different geometry and the range of control parameters.

We now compare our experimental results with some model predictions. The predictions of the thermal convection model proposed by Grossmann & Lohse (2000, 2001, 2002) agree very well with many experimental results of the scaling behaviour of $Re(Ra, Pr)$ and $Nu(Ra, Pr)$. This model decomposes both the thermal and viscous dissipations into the contributions of boundary layers and those of the bulk. According to this assumption, they have four regimes corresponding to different

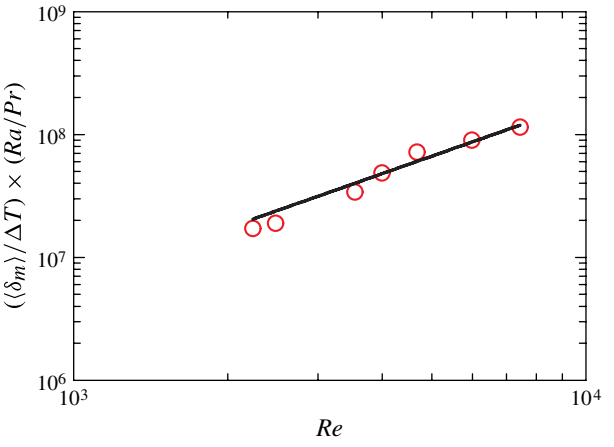

FIGURE 12. (Colour online) The measured $(\langle\delta\rangle/\Delta T) \times (Ra/Pr)$ as a function of Re. The solid line is a power law fitting to the data yielding the relation $(\langle\delta_m\rangle/\Delta T) \times (Ra/Pr) = 250Re^{1.5\pm0.1}$.

scaling relationships. Our experiment lies in the regime IV_u of the (Ra, Pr) phase diagram of the GL model, which basically assume that the thermal dissipations and viscous dissipations are both bulk dominated and the viscous boundary layer is thicker than the thermal boundary layer (Grossmann & Lohse 2000). The predicted relation of Re with respect to Ra and Pr is

$$Re = 0.16Ra^{4/9}Pr^{-2/3}. \tag{3.6}$$

Comparing this result with our experimental results, i.e. $Re = 0.13Ra^{0.43\pm0.01}$, we see that the Ra number scaling of the present result is in good agreement with the model prediction. However, we note that if we substitute $Pr = 19.4$ into (3.6), we have $Re = 0.02Ra^{4/9}$, which is not consistent with present result.

A recent model of the LSC proposed by Brown & Ahlers (2007, 2008) can explain most of the observed features of the LSC. They use two ordinary differential equations, one for the flow strength δ and the other for azimuthal orientation θ of the LSC, which are the quantities that can be measured directly using the multithermal probe technique, to model the dynamics of the LSC. One important prediction of the model is the relation between the normalized flow strength of the LSC with Re, which is

$$\frac{\langle\delta\rangle}{\Delta T} \times \frac{Ra}{Pr} = 18\pi Re^{3/2}. \tag{3.7}$$

Figure 12 shows the measured $(\langle\delta_m\rangle/\Delta T) \times (Ra/Pr)$ as a function of Re for the high-Pr regime. The circles are experimental data and the solid line is a power law fitting attempted to the data which yields

$$\frac{\langle\delta_m\rangle}{\Delta T} \times \frac{Ra}{Pr} = 250Re^{1.5\pm0.1}. \tag{3.8}$$

We can see that the experimental result of the Re scaling exponent is in good agreement with the model prediction. We note that the prefactor of our result is four times larger than the model prediction and twice as large as that reported by

Brown & Ahlers (2008). For the discrepancy of the prefactor between the model and experiments, we have no explanation.

3.4. *Cessations, reversals, flow mode transitions, torsional and sloshing oscillations*

Cessation of the LSC means that the flow strength during a period drops to zero. It has been shown by Xi & Xia (2007) that during a cessation process, the LSC decoheres from an organized structure to a very chaotic flow. Flow cessations have been observed in several experimental studies. Xi & Xia (2008*a*) carried out measurements of the dynamics of the LSC using water as the working fluid at $Pr = 5.3$ and convection cells with aspect ratio $\Gamma = 1$ and 0.5, respectively. They observed cessation events in both aspect ratio cells and their results show that cessation events are much more likely to occur for a convection cell with aspect ratio $\Gamma = 0.5$. Ahlers *et al.* (2009*a*) made measurements of the dynamics of the LSC in a convection cell with aspect ratio $\Gamma = 0.5$ using compressed gas at $Pr = 0.67$ as the working fluid. They also observed momentary vanishings of the flow strength. However, since the duration of these events are much longer than the typical time scale of the system, say the LSC turnover time τ_0, they do not regard these as cessations. Using water as the working fluid with $Pr = 4.3$ and a convection cell with aspect ratio unity, Brown & Ahlers (2006*b*) found that the cessation frequency of the LSC does not depend on Ra.

As the previous studies focus on low and moderate Pr, a natural question is will the cessation events exist in high-Pr RB convection? If so, will cessations be more or less likely to happen? Will there be any Ra dependence of the cessation frequency? Our experiments using water at $Pr = 7.8$ and FC77 at $Pr = 19.4$ as the working fluids can partially answer these questions.

For ease of data analysis, in the present paper we adopt the criteria used by Xi & Xia (2007) to define a cessation event. That is, the flow strength δ_i drops to 15 % of the corresponding mean value $\langle \delta_i \rangle$. Several threshold values from 10 to 30 % of the mean value were tried in the analysis and they all gave the same statistical results. Unless stated otherwise, hereafter we require that the flow amplitude at the three heights of the LSC drop to 15 % of the corresponding mean value simultaneously for a cessation event. Figure 13 shows an example of the cessation event found in the long-time series (∼700 h) measured at $Ra = 2.0 \times 10^{11}$ and $Pr = 19.4$. From top to bottom, the azimuthal orientation θ_i, the flow strength δ_i, schematic drawing of the flow inside the convection cell and the enlargement of the cessation part are shown respectively.

One could see from the figure that during the cessation, there are several stages. At the very beginning (time = 0 s), the LSC is a single-roll structure whose direction is clockwise (figure 13*c*(1)). Then it begins to become weaker and weaker. At ∼280 s, the LSC loses its coherence and finally cannot be identified (figure 13*c*(2)). This fading process only lasts for ∼40 s (figure 13*d*), which is of the same order as the time it takes for the LSC to have one turn. Then the thermal plumes are trying to reorganize into a coherent structure. During this stage, the LSC is unstable. From the figure, we see that a roll which has the size larger than half of the convection cell emerges at the top part of the convection cell at ∼400 s (figure 13*c*(3)). Since it is not stable, ∼240 s later this roll is replaced by another roll which lies at the bottom part of the cell (figure 13*c*(4)). Then after 240 s the LSC rebuilds itself into a single-roll structure which occupies the whole convection cell and has the same direction as that of the LSC before cessation event happens (figure 13*c*(5)). As we can see that after a cessation event, the LSC recovers to its former state without reverse of the flow direction.

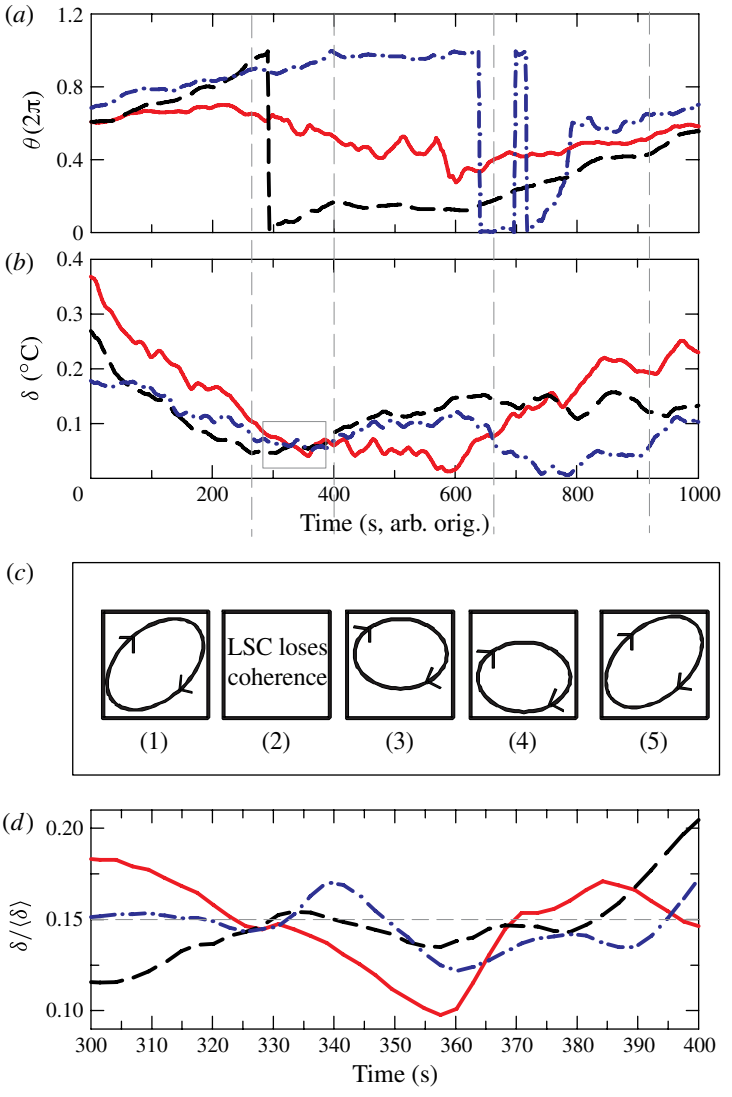

FIGURE 13. (Colour online) Example of a cessation event ($Ra = 2.0 \times 10^{11}$ and $Pr = 19.4$). (*a*) The orientation and (*b*) the flow strength during the cessation process. (*c*) Schematic drawing of the flow configuration. (*d*) An enlargement of the normalized flow strength during cessation as shown in (*b*) with a small grey rectangle. In (*a,b,d*), the dash-dotted, dashed and solid lines are the corresponding quantities measured from the top, middle and bottom heights of the LSC, respectively. The short dashed line in (*d*) corresponds to 15 % $\langle\delta\rangle$.

In the above analysis, we see that the flow strength of the LSC at three different heights, namely top middle and bottom, are all below the threshold values. This ensures that there is no coherent flow at the time period (see figure 13*d*). Using a convection cell with aspect ratio one half, Xi & Xia (2007) reported that they have identified 1813, 1855 and 1798 cessation events from the 34-day data for the top, middle and bottom heights of thermistors, respectively, at $Ra = 5.6 \times 10^{10}$ and $Pr = 5.0$. For the results reported by Xi & Xia (2007), although the authors are of the idea that

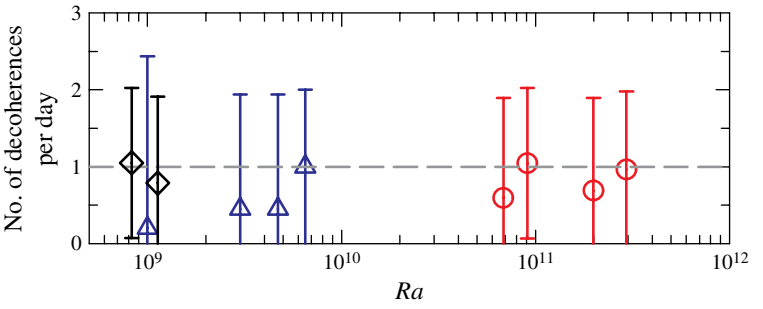

FIGURE 14. (Colour online) Decoherence frequency as a function of Ra for different Pr. Circles $Pr = 19.4$ and diamonds $Pr = 7.8$ (this work); triangles $Pr = 5.3$ (Xi *et al.* 2006). The dashed line is the averaged value of all of the data.

for a cessation the flow strength at the three heights should be below the threshold value simultaneously, the statistical results of the paper is mainly based on the data obtained at the mid-height. Recently Weiss & Ahlers (2011) reported measurements of the dynamics of LSC in a cell with aspect ratio one half and they found that the cessations, which satisfy the criteria that the flow strength at three different heights go below the threshold value at the same time, is ∼0.25 times per day with very large errors (Weiss & Ahlers 2011). It is quite obvious that these two experiments do not agree with each other. It was discovered later by Xi & Xia (2008*b*) that there are complex flow mode transitions exist in a convection cell with aspect ratio one half. Thus, we suggest that most of the cessations found by Xi & Xia (2007) actually involve these complex flow mode transitions. Applying the same criteria for cessation to present data measured at $Ra = 2.0 \times 10^{11}$ and $Pr = 19.4$, only 3 cessations are observed in a time period of 700 h, which corresponds to 0.1 times per day. Owing to the limited number of occurrences of cessation, we will not discuss the Ra and Pr dependence of the cessation rate, which satisfies the above criteria.

The 'cessation' counted only at the a certain height of the LSC indicates that the LSC at this time period loses its coherence and that it is not a well-defined single-roll structure. We define these 'cessations' counted at one height of the LSC as decoherences. The measured decoherence frequency (number of decoherences per day) as a function of Ra at different Pr is shown in figure 14. The Ra is from 8.3×10^8 to 2.9×10^{11}, and Pr is from 5.3 to 19.4. Each of these measurements at different Ra and Pr lasts at least 50 h. The diamonds are experimental results at $Pr = 7.8$, circles are experimental results at $Pr = 19.4$ and triangles are experimental results from Xi *et al.* (2006) at $Pr = 5.3$. It is clear that there is no apparent Ra dependence of the decoherence frequency, which is of order one. This means that the LSC loses its coherence once a day on average. Brown & Ahlers (2006*b*) reported that the cessation frequency of the LSC has no Ra dependence and has a mean rate of 1.5 times per day using water as the working fluid at $Pr = 4.3$. However, it is not clear to us what criteria was used in that work. If they also count cessation frequency only based on data at the mid-height, we see good agreements between two experiments. From figure 14, it is also clear that the Pr dependence of the decoherence frequency is very weak. This can be seen more clearly in figure 15, where we plot the averaged decoherence frequency for different Ra at a fixed Pr as a function of Pr.

Taken together, decoherences counted at the mid-height in three-dimensional (3D) turbulent RB convection appear to be independent of both Ra and Pr. The cessations

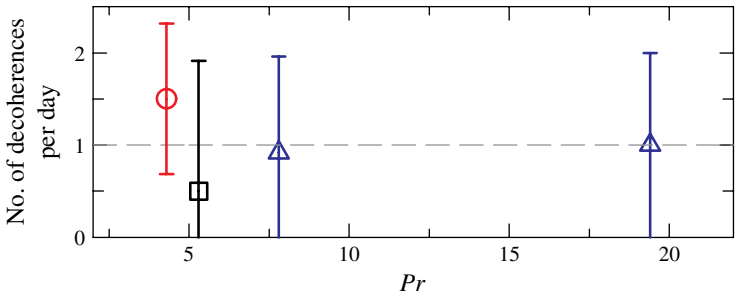

FIGURE 15. (Colour online) Decoherence frequency as a function of Pr. Circles: data from Brown & Ahlers (2006*b*); squares: data from Xi *et al.* (2006); and triangles: data from the current article. The dashed line is the averaged value of all of the data.

that require flow strength at the three different heights go below the threshold value simultaneously are quite rare. This is rather different from the 2D or quasi-2D case, as shown by the numerical and experimental study of Sugiyama *et al.* (2010). In that work, it was found that in 2D turbulent RB convection, cessations always lead to reversals of the LSC and that the rate of cessation has strong dependence on both Ra and Pr.

Flow reversal and also flow mode transitions are found but very rare in the present high-Pr turbulent RB convection. The torsional and sloshing oscillations of the LSC were also identified from the power spectra of the measured temperatures along the sidewall and the azimuthal orientation θ of the LSC. The results related to flow mode transitions, flow reversals as well as torsional and sloshing oscillations are the same at the high Pr as those of moderate Pr. Thus, we placed them in the appendices to make the paper more focused on the differences between the two Pr regimes rather than repeating similar analysis.

4. Conclusion

We have made the first systematic experimental study of the dynamics of the LSC in turbulent RB convection at the high-Pr regime. With water and FC77 as the working fluids, studies of flow dynamics were made at $Pr = 7.8$ and 19.4, respectively. Using a sidewall with small hollow cylinders as thermistor holders, the horizontal temperature profiles of the top, middle and bottom heights of the LSC are measured using the multithermal probe technique. The SF and TEE methods are applied in the data analysis.

We found that the LSC is a single-roll structure most of the time. The cross-correlation functions of the flow strength δ between different heights and those of the azimuthal orientation θ reveal that δ (also θ) at different heights of the LSC are strongly correlated with each other. The p.d.f.s of δ show Gaussian distributions with exponential tails to the left side, which suggests that the cessations and flow reversals, during which δ is relatively small, are more likely to happen than a typical Gaussian process. The p.d.f.s of the orientation show that there is a preferred direction for the LSC which is also reported by Xi *et al.* (2006) using water as the working fluid at moderate Pr.

The azimuthal diffusive motion of the LSC was also observed. It is found that the p.d.f.s of angular speed Ω at the three different heights could be well represented by Gaussian functions, which is consistent with the diffusive motion. However, Ω in

FC77 is approximately two orders of magnitude smaller when compared with that in water. The azimuthal diffusivity obtained at $Pr = 19.4$ and $Ra = 2.0 \times 10^{11}$ is three orders of magnitude smaller than that obtained at $Pr = 4.3$ and $Ra = 2.0 \times 10^{11}$. The auto-correlation functions of Ω at different heights of the LSC reveal that Ω oscillates with the same time period as the turnover time of the LSC. The cross-correlation function of $\Delta\Omega_{tm}$ and $\Delta\Omega_{bm}$ oscillates with a π phase delay, which indicates the existence of the torsional oscillation. The time-averaged non-dimensional angular speed $\langle|\Omega_m|\rangle T_d$ as a function of Ra at $Pr = 19.4$ and 5.3 can be represented by a single power law relation $\langle|\Omega_m|\rangle T_d \propto Ra^{0.36\pm0.1}$.

The Reynolds number Re based on the oscillation of the LSC scales with Rayleigh number Ra as $Re = 0.13Ra^{0.43\pm0.01}$, which is in good agreement with previous experiments done using water, organic fluids (Lam *et al.* 2002) and gas near the liquid gas critical point (Ashkenazi & Steinberg 1999) as the working fluids. Comparing present results with the GL model predictions (Grossmann & Lohse 2000, 2001, 2002), which give a relationship $Re = 0.16Ra^{4/9}Pr^{-2/3}$, we found that present results and the model prediction agree very well with each other for the scaling exponent of Ra. Good agreements in terms of scaling exponents between present experimental results of the normalized flow strength versus Re and that of the LSC model prediction by Brown & Ahlers (2008) were found. The experimental result shows $(\langle\delta_m\rangle/\Delta T) \times (Ra/Pr) = 250Re^{1.5\pm0.1}$ and that of the model prediction is $(\langle\delta\rangle/\Delta T) \times (Ra/Pr) = 18\pi Re^{3/2}$.

The rich dynamical behaviours of the LSC, such as cessations, flow reversals and flow mode transitions are also observed in the high-Pr RB convection. The cessation rate, which requires the flow strength at the three heights to all fall below a threshold value simultaneously, is quite low. However, if we consider the strength at the mid-height only, the obtained decoherence rate then appears to be independent of both Ra and Pr within the resolution of the experiment. The torsional and sloshing oscillations are observed from the power spectra of the orientations and those of the off-centre distance, respectively.

Acknowledgements

We thank H.-D. Xi for suggestions on the design of the convection cell, R. Ni and S.-D. Huang for many helpful discussions. This work is supported in part by the Hong Kong Research Grants Council (RGC) under grant numbers CUHK 403811 and CUHK 404409; and in part by a RGC Direct Grant (project code: 2060441).

Appendix A. Flow reversals and flow mode transitions

A.1. *Flow reversals*

We show two kinds of flow reversals, namely the reorientation-led and cessation-led flow reversals in figure 16. For the reorientation-led reversal (*a*,*c*), it is seen that the LSC goes through a fast change of the azimuthal orientation by π in $\sim$300 s ($\sim$10 times of τ_0). Since the reversed direction is not the 'preferred' direction, the LSC goes back to the previous position again. During this process, the amplitudes of the three heights of the LSC remain well above the threshold value. A cessation-led reversal is shown in figure 16(*b*,*d*). As these figure shows, the LSC is a single-roll structure at the beginning, then it starts to become weak and the orientation changes from 0.5 (in units of 2π) to almost 1.0. Then at $\sim$250 s, the LSC recovers from a decoherent state to a coherent flow and the orientation changes about π, which indicates the flow direction of the LSC reverse.

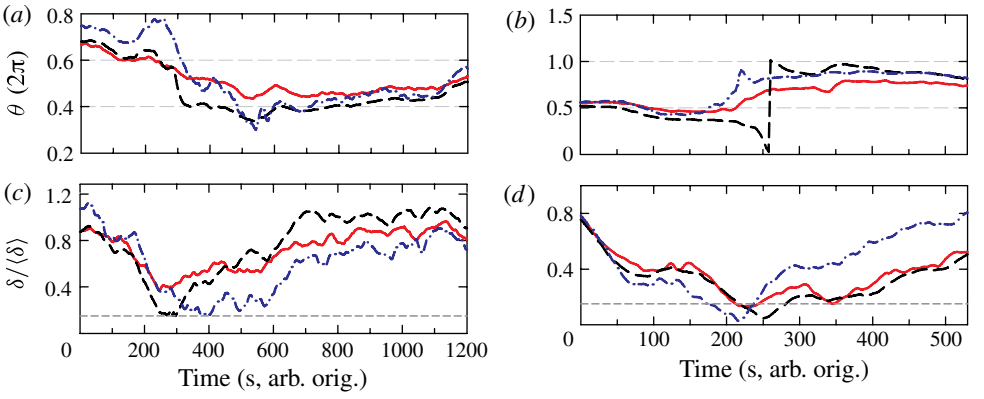

FIGURE 16. (Colour online) Example of reorientation-led flow reversal (*a,c*, $Ra = 2.0 \times 10^{11}$ and $Pr = 19.4$) and cessation-led reversal (*b,d*, $Ra = 3.0 \times 10^{11}$ and $Pr = 19.4$). (*a,b*) The orientation of the LSC during the reversal process. (*c,d*) The corresponding normalized flow strength of the LSC. In both figures, the dash-dotted, dashed and solid lines are the corresponding quantities measured from the top, middle and bottom heights of the LSC respectively. The short dashed lines in (*c,d*) correspond to 15 % $\langle\delta\rangle$.

A.2. *Flow mode transitions*

An example of the SRM–DRM–SRM transitions as discovered by Xi & Xia (2008*b*) is shown in figure 17. At the origin, the LSC is a single roll with clockwise direction. At ∼200 s, the flow strength of the LSC begins to decline. Then at 400 s, the bottom part of the LSC disappears while the top and middle parts of the LSC are well defined and above zero. During the time 400–500 s, the orientations of the top and middle heights of the LSC are in phase with each other while the top height is out of phase with the others. At the same time, the flow strength of different heights is non-zero. This indicates that there is a convection roll, which occupies the upper two thirds of the volume of the cell. Possibly there is a small roll (indicated by the dashed line in figure 17*c*) at the bottom of the cell, since δ_b is non-zero at this stage. At ∼600 s, the LSC rebuilds itself and becomes a single roll again.

Appendix B. Torsional and sloshing oscillations of the LSC

B.1. *Torsional oscillation of LSC*

The torsional oscillation of the LSC is revealed by the peaks of the measured power spectrum of temperature signals as well as the azimuthal orientation θ of the LSC which is shown in figure 18. From these power spectra, a peak located at $\sim 3.3 \times 10^{-2}$ Hz (shown by the grey dashed lines in the figure) is observed. This low-frequency oscillation is the same as that found by Xi *et al.* (2009). Their results show that the origin of this oscillation is the torsional and sloshing motions of the LSC. We also show the coherence power spectrum between θ_t and θ_b as inset of figure 18(*d*). The sharp peak of the coherence spectrum indicates that the top and bottom parts of the LSC oscillate with the same frequency. This characteristic oscillation exists for the *Ra* and *Pr* covered in the present experiments.

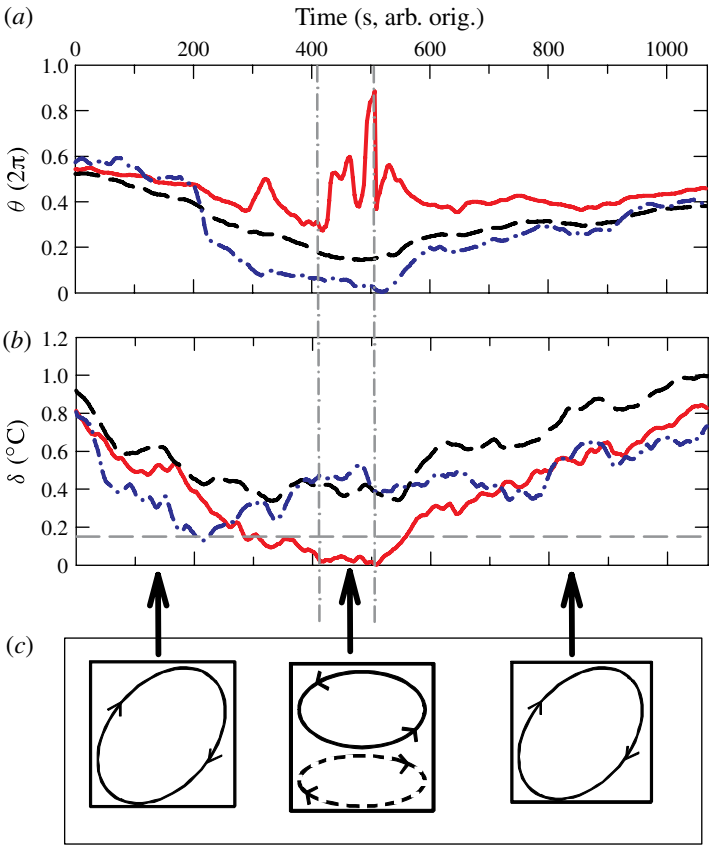

FIGURE 17. (Colour online) Example of the SRM–DRM–SRM transition ($Ra = 2.0 \times 10^{11}$ and $Pr = 19.4$). (*a*) The orientation of the LSC during the SRM–DRM–SRM transition process. (*b*) The corresponding normalized flow strength of the LSC. In both figures, the dash-dotted, dashed and solid lines are the corresponding quantities measured from the top, middle and bottom heights of the LSC, respectively. (*c*) Schematic drawing of the flow configuration of the LSC at different stages. The short dashed line in (*b*) represents the threshold value for cessation events.

B.2. *Sloshing oscillation of LSC*

The sloshing oscillation of the LSC is characterized by the oscillation of the off-centre distance d of the line connecting the hot ascending and cold descending plumes of the LSC. This off-centre distance is obtained using the TEE method described in § 2.

Figure 19 shows the power spectra of the off-centre distance of top, middle and bottom heights of the LSC. It is seen that the power of the middle height has a small peak located at the same position as that of the temperature profiles measured along the sidewall while the peak is almost invisible for the top and bottom heights. This is because the torsional oscillation of the top and bottom heights of the LSC will cancel each other at the middle height. Thus, the sloshing motion could be revealed from the power spectrum at the middle height. For the top and bottom heights, the sloshing oscillations of the LSC are compressed by the strong torsional oscillations, thus the power spectra of the top and bottom heights of the LSC show a very small peak.

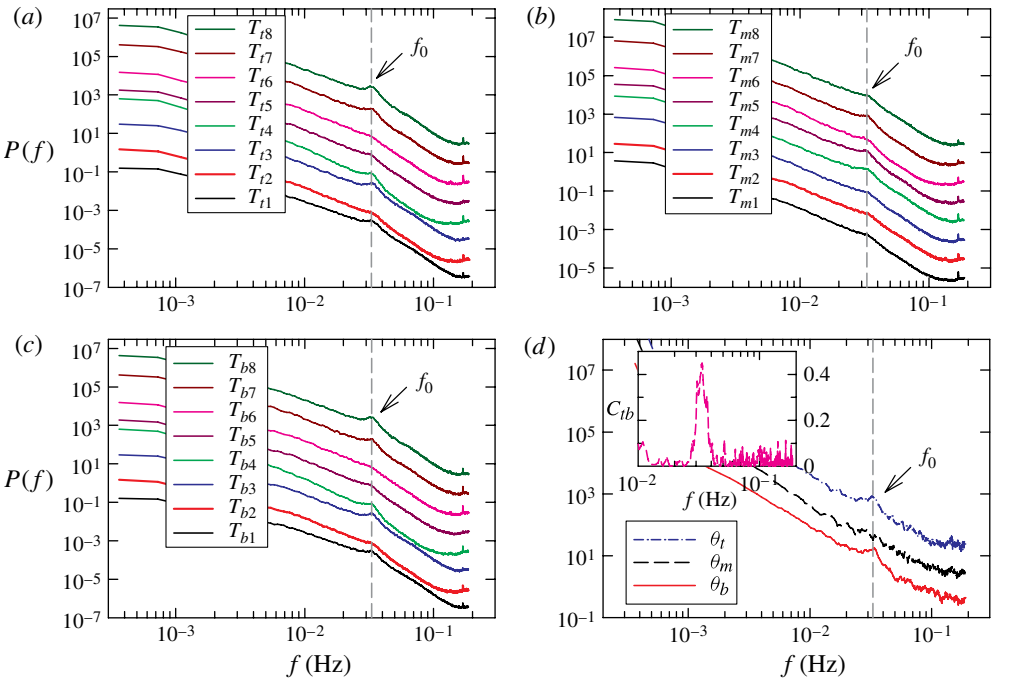

FIGURE 18. (Colour online) Power spectra of the horizontal temperature profiles measured at the (*a*) top, (*b*) middle and (*c*) bottom heights of the LSC; (*d*) power spectra of the orientation of the LSC. The inset of (*d*) is the coherence power spectrum between θ_t and θ_b ($Ra = 2.0 \times 10^{11}$ and $Pr = 19.4$). For clarity, the different curves are shifted upward from each other by a factor of 10 .

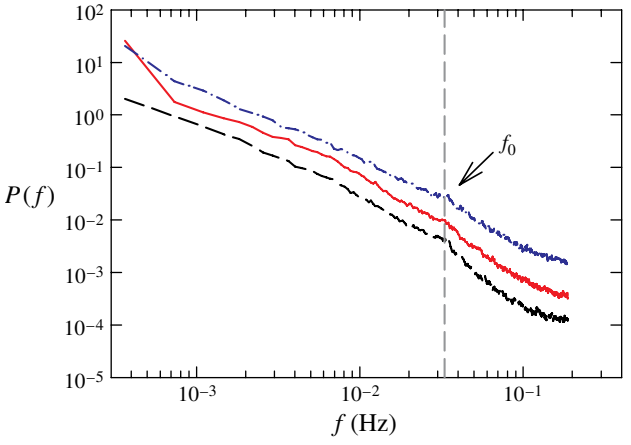

FIGURE 19. (Colour online) Power spectra of the off-centre distances of the top (dashed dot line) middle (dashed line) and bottom (solid line) heights of the LSC ($Ra = 2.0 \times 10^{11}$ and $Pr = 19.4$).

REFERENCES

AHLERS, G., BODENSCHATZ, E., FUNFSCHILLING, D. & HOGG, J. 2009*a* Turbulent Rayleigh–Bénard convection for a Prandtl number of 0.67. *J. Fluid Mech.* **641**, 157–167.

AHLERS, G., GROSSMANN, S. & LOHSE, D. 2009*b* Heat transfer and large-scale dynamics in turbulent Rayleigh–Bénard convection. *Rev. Mod. Phys.* **81**, 503–537.

ASHKENAZI, S. & STEINBERG, V. 1999 High Rayleigh number turbulent convection in a gas near the gas–liquid critical point. *Phys. Rev. Lett.* **83**, 3641–3644.

BENZI, R. 2005 Flow reversal in a simple dynamical model of turbulence. *Phys. Rev. Lett.* **95**, 024502.

BROWN, E. & AHLERS, G. 2006*a* Effect of the Earth's Coriolis force on the large-scale circulation of turbulent Rayleigh–Bénard convection. *Phys. Fluids* **18** (12), 125108.

BROWN, E. & AHLERS, G. 2006*b* Rotations and cessations of the large-scale circulation in turbulent Rayleigh–Bénard convection. *J. Fluid Mech.* **568**, 351–386.

BROWN, E. & AHLERS, G. 2007 Large-scale circulation model for turbulent Rayleigh–Bénard convection. *Phys. Rev. Lett.* **98**, 134501.

BROWN, E. & AHLERS, G. 2008 A model of diffusion in a potential well for the dynamics of the large-scale circulation in turbulent Rayleigh–Bénard convection. *Phys. Fluids* **20** (7), 075101.

BROWN, E., FUNFSCHILLING, D. & AHLERS, G. 2007 Anomalous Reynolds-number scaling in turbulent Rayleigh–Bénard convection. *J. Stat. Mech.* 10005.

BROWN, E., NIKOLAENKO, A. & AHLERS, G. 2005 Reorientation of the large-scale circulation in turbulent Rayleigh–Bénard convection. *Phys. Rev. Lett.* **95**, 084503.

CASTAING, B., GUNARATNE, G., HESLOT, F., KADANOFF, L., LIBCHABER, A., THOMAE, S., WU, X.-Z., ZALESKI, S. & ZANETTI, G. 1989 Scaling of hard thermal turbulence in Rayleigh–Bénard convection. *J. Fluid Mech.* **204**, 1–30.

CIONI, S., CILIBERTO, S. & SOMMERIA, J. 1997 Strongly turbulent Rayleigh–Bénard convection in mercury: comparison with results at moderate Prandtl number. *J. Fluid Mech.* **335**, 111–140.

FUNFSCHILLING, D. & AHLERS, G. 2004 Plume motion and large-scale circulation in a cylindrical Rayleigh–Bénard cell. *Phys. Rev. Lett.* **92**, 194502.

GROSSMANN, S. & LOHSE, D. 2000 Scaling in thermal convection: a unifying theory. *J. Fluid Mech.* **407**, 27–56.

GROSSMANN, S. & LOHSE, D. 2001 Thermal convection for large Prandtl numbers. *Phys. Rev. Lett.* **86**, 3316–3319.

GROSSMANN, S. & LOHSE, D. 2002 Prandtl and Rayleigh number dependence of the Reynolds number in turbulent thermal convection. *Phys. Rev.* E **66**, 016305.

KACZOROWSKI, M., SHISHKINA, O., SHISHKIN, A., WAGNER, C. & XIA, K.-Q. 2011 Analysis of the large-scale circulation and the boundary layers in turbulent Rayleigh–Bénard convection. In *Direct and Large-Eddy Simulation VIII* (ed. H. Kuerten, B. Geurts, V. Armenio & J. Frhlich), vol. 15, pp. 383–388. Springer.

LAM, S., SHANG, X.-D., ZHOU, S.-Q. & XIA, K.-Q. 2002 Prandtl number dependence of the viscous boundary layer and the Reynolds numbers in Rayleigh–Bénard convection. *Phys. Rev.* E **65**, 066306.

NIEMELA, J. J., SKRBEK, L., SREENIVASAN, K. R. & DONNELLY, R. J. 2001 The wind in confined thermal convection. *J. Fluid Mech.* **449**, 169–178.

QIU, X.-L. & TONG, P. 2001 Large-scale velocity structures in turbulent thermal convection. *Phys. Rev.* E **64**, 036304.

SANO, M., WU, X.-Z. & LIBCHABER, A. 1989 Turbulence in helium-gas free convection. *Phys. Rev.* A **40**, 6421–6430.

SHANG, X.-D. & XIA, K.-Q. 2001 Scaling of the velocity power spectra in turbulent thermal convection. *Phys. Rev.* E **64**, 065301.

SUGIYAMA, K., NI, R., STEVENS, R. J. A. M., CHAN, T. S., ZHOU, S.-Q., XI, H.-D., SUN, C., GROSSMANN, S., XIA, K.-Q. & LOHSE, D. 2010 Flow reversals in thermally driven turbulence. *Phys. Rev. Lett.* **105**, 034503.

SUN, C., XI, H.-D. & XIA, K.-Q. 2005*a* Azimuthal symmetry, flow dynamics, and heat transport in turbulent thermal convection in a cylinder with an aspect ratio of 0.5. *Phys. Rev. Lett.* **95**, 074502.

SUN, C. & XIA, K.-Q. 2005 Scaling of the Reynolds number in turbulent thermal convection. *Phys. Rev.* E **72**, 067302.

SUN, C. & XIA, K.-Q. 2007 Multi-point local temperature measurements inside the conducting plates in turbulent thermal convection. *J. Fluid Mech.* **570**, 479–489.

SUN, C., XIA, K.-Q. & TONG, P. 2005*b* Three-dimensional flow structures and dynamics of turbulent thermal convection in a cylindrical cell. *Phys. Rev.* E **72**, 026302.

TAKESHITA, T., SEGAWA, T., GLAZIER, J. A. & SANO, M. 1996 Thermal turbulence in mercury. *Phys. Rev. Lett.* **76**, 1465–1468.

WEISS, S. & AHLERS, G. 2011 Turbulent Rayleigh–Bénard convection in a cylindrical container with aspect ratio $\Gamma = 0.50$ and Prandtl number $\mathrm{Pr} = 4.38$. *J. Fluid Mech.* **676**, 5–40.

XI, H.-D., LAM, S. & XIA, K.-Q. 2004 From laminar plumes to organized flows: the onset of large-scale circulation in turbulent thermal convection. *J. Fluid Mech.* **503**, 47–56.

XI, H.-D. & XIA, K.-Q. 2007 Cessations and reversals of the large-scale circulation in turbulent thermal convection. *Phys. Rev.* E **75**, 066307.

XI, H.-D. & XIA, K.-Q. 2008*a* Azimuthal motion, reorientation, cessation, and reversal of the large-scale circulation in turbulent thermal convection: a comparative study in aspect ratio one and one-half geometries. *Phys. Rev.* E **78**, 036326.

XI, H.-D. & XIA, K.-Q. 2008*b* Flow mode transitions in turbulent thermal convection. *Phys. Fluids* **20** (5), 055104.

XI, H.-D., ZHOU, Q. & XIA, K.-Q. 2006 Azimuthal motion of the mean wind in turbulent thermal convection. *Phys. Rev.* E **73**, 056312.

XI, H.-D., ZHOU, S.-Q., ZHOU, Q., CHAN, T.-S. & XIA, K.-Q. 2009 Origin of the temperature oscillation in turbulent thermal convection. *Phys. Rev. Lett.* **102**, 044503.

XIA, K.-Q. 2011 How heat transfer efficiencies in turbulent thermal convection depend on internal flow modes. *J. Fluid Mech.* **676**, 1–4.

XIA, K.-Q., LAM, S. & ZHOU, S.-Q. 2002 Heat-flux measurement in high-Prandtl-number turbulent Rayleigh–Bénard convection. *Phys. Rev. Lett.* **88**, 064501.

ZHOU, Q., XI, H.-D., ZHOU, S.-Q., SUN, C. & XIA, K.-Q. 2009 Oscillations of the large-scale circulation in turbulent Rayleigh–Bénard convection: the sloshing mode and its relationship with the torsional mode. *J. Fluid Mech.* **630**, 367–390.

ZHOU, S.-Q., SUN, C. & XIA, K.-Q. 2007 Measured oscillations of the velocity and temperature fields in turbulent Rayleigh–Bénard convection in a rectangular cell. *Phys. Rev.* E **76**, 036301.